

Thin-shell approximation of Mie theory for a thin anisotropic layer spaced away from a spherical core: Application to dye-coated nanostructures

Chhayly Tang ,* Baptiste Auguié , and Eric C. Le Ru [†]

The MacDiarmid Institute for Advanced Materials and Nanotechnology, School of Chemical and Physical Sciences, Victoria University of Wellington, PO Box 600, Wellington 6140, New Zealand

 (Received 7 June 2021; accepted 25 August 2021; published 3 September 2021)

We here develop a thin-shell approximation of the Mie scattering problem for a spherical multilayer structure consisting of central core, a spacer layer, and a thin layer with radially anisotropic dielectric function. This thin layer can, for example, represent a uniform layer of adsorbed dyes at a fixed distance from a spherical nanoparticle, with an effective anisotropic dielectric tensor to account for dye-orientation effects. This geometry with the spacer layer was recently shown to be necessary to precisely account for all electromagnetic effects in such systems [C. Tang, B. Auguié, and E. C. Le Ru, *Phys. Rev. B* **103**, 085436 (2021)]. The Mie theory solution involves Bessel functions of complex order, which are not commonly available in many numerical calculations. We show that this hurdle is overcome in the thin-shell approximation, where the solution is of similar complexity to that of isotropic Mie theory with only spherical Bessel functions of integer order. We also apply this approximation to the calculation of the optical absorption in each individual layer. Using the dye-on-metal-nanoparticle system as illustration, we show that the thin-shell predictions agree extremely well with the full solution for experimentally relevant parameters, and can therefore be used instead. This speeds up the numerical implementation and will simplify further analytical developments.

DOI: [10.1103/PhysRevA.104.033502](https://doi.org/10.1103/PhysRevA.104.033502)

I. INTRODUCTION

Mie theory provides the full solution of the electromagnetic scattering problem by a sphere [1,2] or a spherical multilayer [3,4]. Because it is analytic, and easily implemented numerically, it is one of the most used tools to predict the optical properties of particles, nanoparticles (NPs), and NPs coated with molecules. These calculations are particularly relevant to the field of plasmonics, which studies and exploits the unique interaction of light with noble metals [5,6], with diverse applications in, for example, sensing [7–10] or surface-enhanced Raman and fluorescence spectroscopy [11]. Much experimental and theoretical work has recently focused on understanding the interaction between plasmon and dye resonances in dye-on-metal-NP systems [12–19], with particular interest in the strong-coupling regime [20–22]. Many of these phenomena are first modeled for spheres using Mie theory. Shape effects can then be investigated separately using more elaborate tools such as finite-element modeling [23,24].

Although less common, it is also possible to generalize Mie theory to radially anisotropic media, where the dielectric function of the material is different for the radial and tangential directions. This has been used to study the influence of anisotropy on the plasmon resonances of metallic nanoparticles [25,26]. It is also particularly relevant to dye-on-NPs systems, where the preferred adsorbed dye orientation often result in a strongly anisotropic optical response [27,28], which cannot be modeled with isotropic Mie theory. A general

theory of anisotropic Mie scattering for an optically isotropic particle surrounded by an anisotropic shell was given by Roth and Dignam [29], who also derived an effective dielectric tensor to account for the anisotropic response resulting from a layer of adsorbed dyes with fixed orientation. This model was further refined to account for image dipole effects for dyes adsorbed on a metallic nanoparticle at a fixed distance d from the surface [30,31]. This was recently further developed and extended to the more experimentally relevant case of dye-on-NP embedded in a dielectric medium such as water [32]. Combined with anisotropic Mie theory, the resulting one-layer effective-medium model (EMM), see Fig. 1(a), was compared to the full microscopic solution obtained from generalized coupled-dipole calculations [33,34]. By choosing the shell thickness as $l_s = 2d$, a reasonable agreement was obtained, but some discrepancies remained, in particular, for a tangential orientation of dyes [32]. To overcome these issues, the authors of Ref. [32] proposed an improved two-layer EMM where a spacer layer of thickness $d - l_s/2$ was introduced between the core and the anisotropic dye layer, see Fig. 1(b). The main advantage of this two-layer EMM is that the dye shell thickness l_s can be defined independently of the distance d from the dye molecules to the NP surface. The first can then be chosen to be very small to ensure the results do not depend on its choice. As shown in Ref. [32], the two-layer EMM then results in much improved agreement with the microscopic solution.

Another benefit of a small l_s in the two-layer EMM is that the solution should then be accurately approximated by that in the limit of a vanishing l_s , which we call the thin-anisotropic-shell approximation (TASA). This approach was first used by Lange and Aragon [35] in the special case of bubbles (where

*chhayly.tang@vuw.ac.nz

[†]eric.leru@vuw.ac.nz

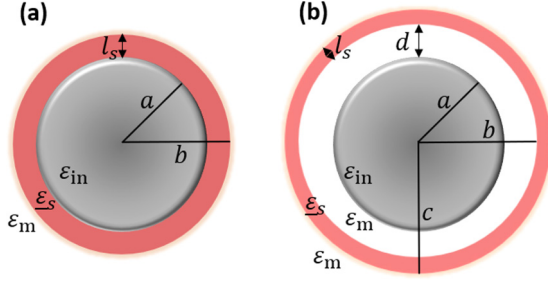


FIG. 1. Schematic of the scatterer structure (a) previously studied one-layer core-shell structure and (b) the improved two-layer core-spacer-shell model.

the spherical core is the same as the embedding medium), and was generalized to an arbitrary isotropic-core-anisotropic-shell system [36]. The latter can, for example, be applied to the one-layer EMM but only if the shell thickness $l_s = 2d$ is small enough [36]. The main advantage of these TASA solutions is that they no longer include the complex-order Bessel functions that arise in the full solutions of anisotropic systems [29]. These complex-order Bessel functions complicate numerical implementations and dramatically increase computation times. In contrast, the TASA solutions require only the same integer-order spherical Bessel functions as in standard Mie theory.

In this work, we derive the TASA solution of the two-layer (core-spacer-anisotropic shell) problem. As for previous TASA solutions, only integer-order spherical Bessel functions are needed in this approximation. The validity of this new TASA solution is demonstrated by comparing its predictions to the full solutions. This is illustrated in the model case of silver NPs coated with radially or tangentially oriented dye molecules. The EMM of Ref. [32] is used to describe the anisotropic response of the dye layer. The shell thickness in the two-layer EMM can be chosen arbitrarily small, in contrast to previous TASA solutions where it was imposed by physical parameters (for example, $l_s = 2d$ in the one-layer EMM). At very small l_s , excellent agreement is demonstrated between the TASA and the full isotropic Mie solution. We conclude that the simpler and more efficient TASA solution can be routinely used in such calculations. Finally, we also extend these results to predict the optical absorption in the anisotropic dye layer. Previous studies of anisotropic Mie theory have all focused on the optical properties of the entire system (core + shell), but absorption in the shell only (or core only) may be more relevant to some applications, for example, plasmonic-enhanced photobleaching [37] or photo-induced catalysis [38]. For an isotropic system, the internal absorption cross section in each spherical layer was derived by Mackowski *et al.* [39]. We here generalize these results to include anisotropic layers and explain how these can be computed in the TASA solution.

II. MIE THEORY FOR A CORE-SPACER-ANISOTROPIC-SHELL SYSTEM

We consider the light scattering problem by a core-spacer-shell structure, as depicted in Fig. 1(b). The core of radius a

is surrounded by a thin spherical shell of thickness $l_s = c - b$, and embedded in a nonabsorbing medium (typically air or water) with dielectric constant ϵ_m . The core and the anisotropic shell are separated by a spacer medium with dielectric constant ϵ_m and thickness $b - a$. The dielectric function of the core is denoted as ϵ_c and assumed to be isotropic. The anisotropic spherical shell is characterized by a dielectric tensor $\underline{\epsilon}_s$, which is assumed diagonal in the spherical basis with ϵ_n and ϵ_t as its normal (radial) and tangential components, respectively. Explicitly, in the spherical basis, $(\hat{r}, \hat{\theta}, \hat{\phi})$:

$$\underline{\epsilon}_s = \begin{pmatrix} \epsilon_n & 0 & 0 \\ 0 & \epsilon_t & 0 \\ 0 & 0 & \epsilon_t \end{pmatrix}. \quad (1)$$

The solution of the problem can be derived similarly to Ref. [29], with an extra boundary condition for the additional layer. We here only summarize the final results, more details are provided in Appendix A. The extinction, absorption, and scattering cross sections take the same form as in Mie theory:

$$C_{\text{ext}} = \frac{2\pi}{k_m^2} \sum_{n=1}^{\infty} (2n+1) \text{Re}(\Gamma_n + \Delta_n), \quad (2)$$

$$C_{\text{sca}} = \frac{2\pi}{k_m^2} \sum_{n=1}^{\infty} (2n+1) (|\Gamma_n|^2 + |\Delta_n|^2), \quad (3)$$

$$C_{\text{abs}} = C_{\text{ext}} - C_{\text{sca}}, \quad (4)$$

where $k_m = 2\pi\sqrt{\epsilon_m}/\lambda$. Γ_n and Δ_n are the Mie scattering coefficients, which are functions of the size parameters $x = k_m c$, $y = k_m b$, and $z = k_m a$, of the relative indices of refraction $s_c = \sqrt{\epsilon_c}/\sqrt{\epsilon_m}$ and $s_t = \sqrt{\epsilon_t}/\sqrt{\epsilon_m}$, and of the ratio ϵ_t/ϵ_n .

The Mie scattering coefficients are derived as

$$\Gamma_n = -\frac{N_{1n}}{D_{1n}}, \quad (5)$$

$$\Delta_n = -\frac{N_{2n}}{D_{2n}}, \quad (6)$$

with

$$N_{1n} = [\psi\psi]_{n,x}^{m,s} ([\chi\psi]_{n,y}^{m,s} + \Gamma_n^{(1)} [\chi\chi]_{n,y}^{m,s}) - [\chi\psi]_{n,x}^{m,s} ([\psi\psi]_{n,y}^{m,s} + \Gamma_n^{(1)} [\psi\chi]_{n,y}^{m,s}), \quad (7)$$

$$D_{1n} = [\psi\xi]_{n,x}^{m,s} ([\chi\psi]_{n,y}^{m,s} + \Gamma_n^{(1)} [\chi\chi]_{n,y}^{m,s}) - [\chi\xi]_{n,x}^{m,s} ([\psi\psi]_{n,y}^{m,s} + \Gamma_n^{(1)} [\psi\chi]_{n,y}^{m,s}), \quad (8)$$

$$N_{2n} = [\psi\psi]_{n,x}^{e,s} ([\chi\psi]_{n,y}^{e,s} + \Delta_n^{(1)} [\chi\chi]_{n,y}^{e,s}) - [\chi\psi]_{n,x}^{e,s} ([\psi\psi]_{n,y}^{e,s} + \Delta_n^{(1)} [\psi\chi]_{n,y}^{e,s}), \quad (9)$$

$$D_{2n} = [\psi\xi]_{n,x}^{e,s} ([\chi\psi]_{n,y}^{e,s} + \Delta_n^{(1)} [\chi\chi]_{n,y}^{e,s}) - [\chi\xi]_{n,x}^{e,s} ([\psi\psi]_{n,y}^{e,s} + \Delta_n^{(1)} [\psi\chi]_{n,y}^{e,s}), \quad (10)$$

where

$$\Gamma_n^{(1)} = -\frac{s_c \psi_n(z) \psi_n'(s_c z) - \psi_n(z) \psi_n'(s_c z)}{s_c \chi_n(z) \psi_n'(s_c z) - \chi_n(z) \psi_n'(s_c z)}, \quad (11)$$

$$\Delta_n^{(1)} = -\frac{s_c \psi_n'(z) \psi_n(s_c z) - \psi_n'(z) \psi_n(s_c z)}{s_c \chi_n'(z) \psi_n(s_c z) - \chi_n'(z) \psi_n(s_c z)}, \quad (12)$$

and

$$\begin{aligned} [\Lambda \Omega]_{n,x}^{m,s} &= s_t \Lambda'_n(s_t x) \Omega_n(x) - \Lambda_n(s_t x) \Omega'_n(x), \\ [\Lambda \Omega]_{n,x}^{e,s} &= s_t \tilde{\Lambda}'_n(s_t x) \Omega'_n(x) - \tilde{\Lambda}'_n(s_t x) \Omega_n(x), \end{aligned}$$

with $\Lambda = \psi$ or χ , and $\Omega = \psi$, χ , or ξ . (13)

ψ_n and χ_n denote the regular and irregular Riccati-Bessel functions of integer order n and $\xi_n = \psi_n + i\chi_n$. The (\prime) refers to their first derivatives. The functions $\tilde{\psi}_n$ and $\tilde{\chi}_n$ are Riccati-Bessel functions of complex order, which are defined as [36]

$$\tilde{\psi}_n(x) \equiv \sqrt{\pi x/2} J_{w(n)+1/2}(x), \quad (14)$$

$$\tilde{\chi}_n(x) \equiv \sqrt{\pi x/2} Y_{w(n)+1/2}(x), \quad (15)$$

$$\tilde{\xi}_n(x) \equiv \tilde{\psi}_n(x) + i\tilde{\chi}_n(x), \quad (16)$$

where

$$w(n) = \sqrt{\frac{1}{4} + \frac{\varepsilon_t}{\varepsilon_n}(n^2 + n)} - \frac{1}{2}. \quad (17)$$

Note that $w(n)$ is, in general, complex and wavelength-dependent. In our numerical implementation, these functions are expressed in terms of a power series as (see Ref. [40], Secs. 9.1.2 and 9.1.10)

$$J_\nu(x) = \left(\frac{x}{2}\right)^\nu \sum_{k=0}^{\infty} \frac{(-1)^k [x/2]^{2k}}{\Gamma(k+1)\Gamma(\nu+k+1)}, \quad (18)$$

$$Y_\nu(x) = \frac{J_\nu(x) \cos(\pi\nu) - J_\nu(x)}{\sin(\pi\nu)}. \quad (19)$$

We calculate the complex Γ functions in MATLAB using Lanczos series approximation [41]. In all our Mie calculations, we used a relatively small number of multipoles, $N_{\max} = 5$, to truncate the Mie series; in fact, the results are almost converged even when using only $N_{\max} = 1$.

III. THIN ANISOTROPIC SHELL APPROXIMATION

In the derivations of the thin anisotropic shell approximation, results from Refs. [35,36] can be used as a guide to derive the TASA for this system. Briefly, we define $\delta = x - y = k_m l_s$ and seek the solution in the limit $\delta \ll x, y$. For this, we perform a Taylor expansion to first order in δ of all the expressions used in the solution, which, after simplification, leads to

$$\Gamma_n(y, \delta) = -\frac{N_{1n}}{D_{1n}} - \delta \left(\frac{N'_{1n} D_{1n} - N_{1n} D'_{1n}}{(D_{1n})^2} \right), \quad (20)$$

$$\Delta_n(y, \delta) = -\frac{N_{2n}}{D_{2n}} - \delta \left(\frac{N'_{2n} D_{2n} - N_{2n} D'_{2n}}{(D_{2n})^2} \right). \quad (21)$$

All values of N and D above are evaluated at $x = y$, explicitly:

$$\begin{aligned} N_{1n}|_{x=y} &= s_t \Gamma_n^{(1)}, \\ D_{1n}|_{x=y} &= s_t (\Gamma_n^{(1)} - i), \\ N'_{1n}|_{x=y} &= s_t (s_t^2 - 1) \psi_n(y) [\psi_n(y) + \Gamma_n^{(1)} \chi_n(y)], \\ D'_{1n}|_{x=y} &= s_t (s_t^2 - 1) \xi_n(y) [\psi_n(y) + \Gamma_n^{(1)} \chi_n(y)]. \end{aligned} \quad (22)$$

$$\begin{aligned} N_{2n}|_{x=y} &= s_t \Delta_n^{(1)}, \\ D_{2n}|_{x=y} &= s_t (\Delta_n^{(1)} - i), \\ N'_{2n}|_{x=y} &= \frac{s_t n(n+1)}{y^2} \left(\frac{\varepsilon_t}{\varepsilon_n s_t^2} - 1 \right) \psi_n(y) [\psi_n(y) + \Delta_n^{(1)} \chi_n(y)], \\ &\quad + s_t (1 - s_t^2) \psi'_n(y) [\psi'_n(y) + \Delta_n^{(1)} \chi'_n(y)], \\ D'_{2n}|_{x=y} &= \frac{s_t n(n+1)}{y^2} \left(\frac{\varepsilon_t}{\varepsilon_n s_t^2} - 1 \right) \xi_n(y) [\psi_n(y) + \Delta_n^{(1)} \chi_n(y)] \\ &\quad + s_t (1 - s_t^2) \xi'_n(y) [\psi'_n(y) + \Delta_n^{(1)} \chi'_n(y)]. \end{aligned} \quad (23)$$

More detailed derivations are given in Appendix B. Bessel functions of complex orders are no longer required in this approximation. We note that for $\delta = 0$ (i.e., zero shell thickness of the dye layer), the expressions of $\Gamma_n(\delta)$ and $\Delta_n(\delta)$ simplify to those of standard Mie theory for the core only, as expected. Also, for $b = a$, the expressions reduce to those previously obtained in the absence of the spacer layer, Eqs. (13) to (16) in Ref. [36]. Furthermore, if we set $\varepsilon_c = \varepsilon_m$ ($s_c = 1$), then these expressions reduce to Eqs. (3.16) to (3.17) in Ref. [35].

It is also worth noting that the TASA solution above can also be used for a composite core (for example, a core composed of a metal NP covered with a dielectric layer). The only change is that $\Gamma_n^{(1)}$ and $\Delta_n^{(1)}$ [Eqs. (11) and (12)] must be replaced by the Mie susceptibility of the composite core, but the TASA solution remains unchanged.

IV. VALIDATION AND APPLICATION

We now illustrate the range of validity and usefulness of this TASA solution by focusing on a specific system: a silver nanosphere of radius $a = 30$ nm (with dielectric function taken from Ref. [11]) coated with a monolayer of dye at a fixed distance d from the surface. The embedding medium is assumed to be water with $\varepsilon_m = 1.7689$. In Ref. [32], the two-layer effective medium model (EMM) was shown to give the best agreement with the microscopic solution. In this case, the spacer thickness is set to $b - a = d - l_s/2$, and l_s can be chosen as small as desired; we here use $l_s = a/100 = 0.3$ nm. We choose a dye coverage of $\rho = 0.01$ nm² and a distance to the surface $d = 1$ nm, but similar conclusions are obtained at other values of ρ and d . Following Ref. [32], the dye uniaxial polarizability is described by a simple Lorentz oscillator model with parameters matching the experimentally measured optical properties of the main absorption peak of rhodamine 6G at 526 nm [42]

$$\alpha_{\text{uni}}(\lambda) = \alpha_\infty + \frac{\alpha_1 \lambda_1}{\mu_1} \left[\frac{1}{1 - \frac{\lambda^2}{\lambda_1^2} - i \frac{\lambda^2}{\lambda_1 \mu_1}} - 1 \right], \quad (24)$$

where $\alpha_\infty = 9.6 \times 10^{-39}$ A² s⁴ kg⁻¹, $\alpha_1 = 5.76 \times 10^{-38}$ A² s⁴ kg⁻¹, $\lambda_1 = 526$ nm, and $\mu_1 = 10^4$ nm. From this, we can deduce the effective anisotropic dielectric tensor of the dye layer for the two important dye orientations: radial (\perp) or tangential (\parallel), see Ref. [32] for details.

We compare in Fig. 2 the results of the full anisotropic Mie theory and the TASA solutions for a dye-coated silver sphere for these two orientations. The absorption, scattering, and

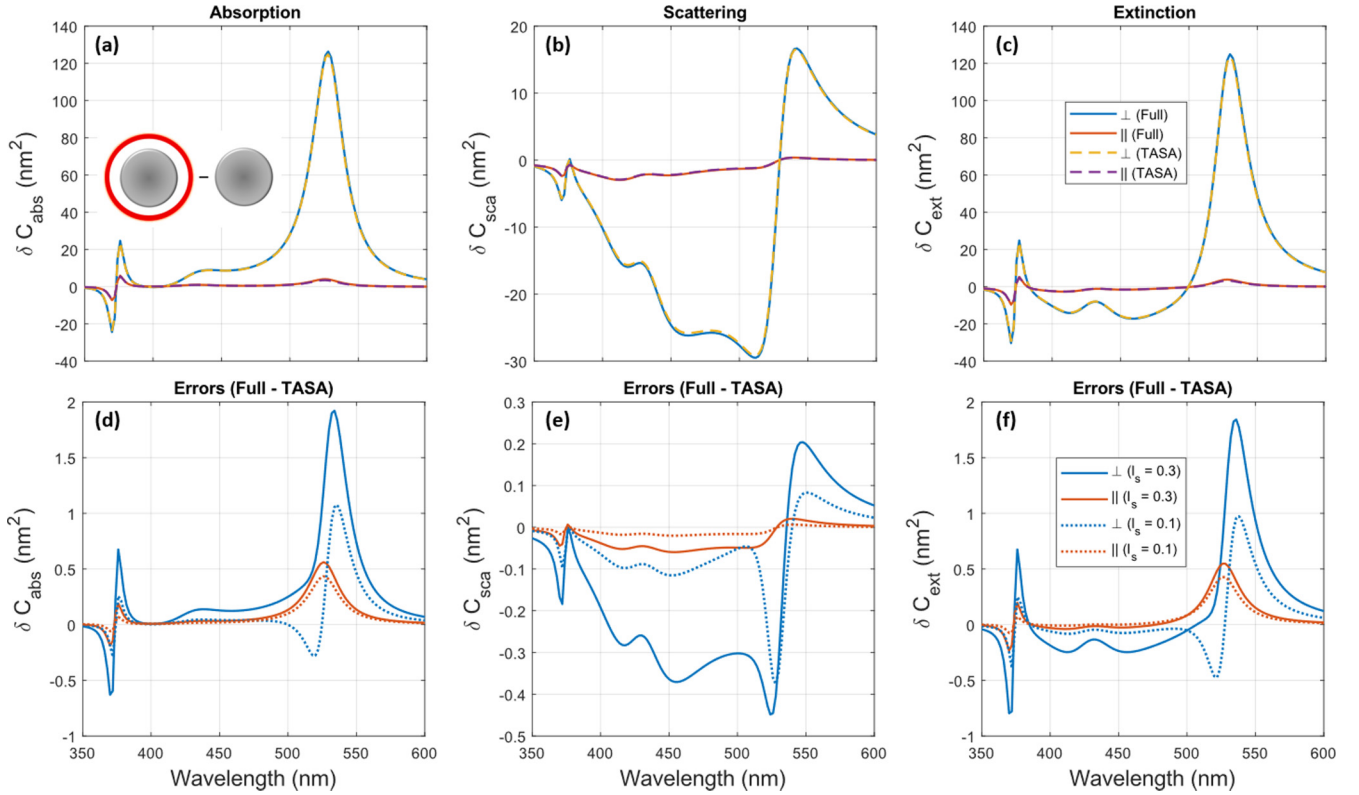


FIG. 2. Mie scattering predictions for a silver sphere of radius $a = 30$ nm in water, coated with a $l_s = 0.3$ nm dye layer with an effective dielectric tensor from Ref. [32] assuming a dye coverage $\rho = 0.01$ nm² and distance from surface $d = 1$ nm. We compare the results of the full anisotropic Mie theory for a two-layer EMM with our TASA for two representative cases: radially oriented (\perp) and tangentially oriented with in-plane isotropy (\parallel) molecules. The panels show the differential cross sections for (a) absorption, (b) scattering, and (c) extinction, and (d)–(f) the corresponding absolute errors between the TASA and exact solutions. The last panels also show the errors for a smaller shell thickness $l_s = 0.1$ nm (dotted lines).

extinction cross sections of the whole system (core + spacer + shell) denoted as C_{abs} , C_{sca} , and C_{ext} , respectively, are not shown as they are strongly dominated by the response of the silver sphere and do not clearly reveal the subtle effects of the shell on the combined system. We therefore focus on the differential cross sections (denoted as δC_{abs} , etc.) instead, which is the difference between the whole system and the core-only cross sections, i.e., $\delta C_{\text{abs}} = C_{\text{abs}} - C_{\text{abs}}^{\text{Bare}}$, for example. The results from the full and TASA solutions are almost indistinguishable in all cases, with errors of the order of a few percent. The errors can be further reduced if desired by decreasing l_s , see Fig. 2. This extremely good agreement (much better than for the one-layer case [36]) can be attributed to the very small shell-thickness l_s . Moreover, l_s can be chosen arbitrarily small to improve accuracy, in contrast to the one-layer TASA where the shell-thickness is imposed by the distance of the dyes from the surface ($l_s = 2d$). More extensive comparisons were carried out (not shown here) and the results confirmed the validity of the TASA with similar errors for shell-thickness l_s of the order of $\sim a/100$.

V. ABSORPTION CROSS SECTIONS

Equations (2) to (4) allow us to compute the differential extinction, scattering, and absorption cross sections of the whole system (core and shells). However, this differential absorption cross sections does not necessarily match the actual

optical absorption in the shell, as the presence of the shell also modifies the electric fields within the core particle and vice versa. Actual absorption in the shell is more relevant to, for example, plasmonic-enhanced photobleaching [37] or photocatalysis [38], where the absorption in a specific region in the system becomes important. To address this issue, we here focus on deriving the internal absorption cross sections in individual layers of a spherical multilayer, with potentially anisotropic response in some layers. We then show that the TASA again provides a simplified, yet accurate, solution in this context.

Mackowski *et al.* [39] derived the internal absorption cross sections for isotropic stratified spheres, which we here generalize to account for radially anisotropic dielectric functions. As for earlier solutions, complex-order Bessel functions \tilde{y}_n and $\tilde{\chi}_n$ must be used, but apart from this change, the expressions are similar to the isotropic case. The electric field in the j th layer is

$$\mathbf{E}(\mathbf{r}) = \frac{\varepsilon_{s,j}}{\varepsilon_{t,j}} E_0 \sum_{n,m} \alpha_{nm}^j \mathbf{M}_{nm}^{(1)}(k_{t,j} \mathbf{r}) + \beta_{nm}^j \tilde{\mathbf{N}}_{nm}^{(1)}(k_{t,j} \mathbf{r}) + \gamma_{nm}^j \mathbf{M}_{nm}^{(2)}(k_{t,j} \mathbf{r}) + \delta_{nm}^j \tilde{\mathbf{N}}_{nm}^{(2)}(k_{t,j} \mathbf{r}), \quad (25)$$

where $s_j = \sqrt{\varepsilon_{t,j}} / \sqrt{\varepsilon_m}$ and α_{nm}^j , β_{nm}^j , γ_{nm}^j and δ_{nm}^j are coefficients that can be determined as described in Appendix A. $\mathbf{M}_{nm}^{(i)}$, $\mathbf{N}_{nm}^{(i)}$ are vector spherical wave functions [43] and $\tilde{\mathbf{M}}_{nm}^{(i)}$, $\tilde{\mathbf{N}}_{nm}^{(i)}$ are their complex-order counterparts. The total

absorption cross section for *all layers* up to the *j*th interface ($r = a_j$) can then be expressed as

$$C_{\text{abs}}(r \leq a_j) = \frac{2\pi}{k_m^2} \text{Re} \left\{ \frac{i}{s_j} \sum_{n=1}^{\infty} (2n+1) \right. \\ \times [\beta_{nm}^j \tilde{\psi}'_n(s_j x_j) + \delta_{nm}^j \tilde{\chi}'_n(s_j x_j)] \\ \times [\beta_{nm}^j \tilde{\psi}_n(s_j x_j) + \delta_{nm}^j \tilde{\chi}_n(s_j x_j)]^* \\ - [\alpha_{nm}^j \psi_n(s_j x_j) + \gamma_{nm}^j \chi_n(s_j x_j)] \\ \left. \times [\alpha_{nm}^j \psi'_n(s_j x_j) + \gamma_{nm}^j \chi'_n(s_j x_j)]^* \right\}, \quad (26)$$

where $x_j = k_m a_j$. From these, the absorption cross section for an individual layer *j* is simply obtained as the difference

$$C_{\text{abs}}^j = C_{\text{abs}}(r \leq a_j) - C_{\text{abs}}(r \leq a_{j-1}). \quad (27)$$

For the special case of the core ($j = 0$), we have $\gamma_{nm}^0 = \delta_{nm}^0 = 0$ and the absorption cross section simplifies to

$$C_{\text{abs}}^{\text{Core}} = \frac{2\pi}{k_m^2} \text{Re} \left\{ \frac{i}{s_c} \sum_{n=1}^{\infty} (2n+1) (|\alpha_{nm}^0|^2 \psi_n(s_c z) [\psi'_n(s_c z)]^* \right. \\ \left. + |\beta_{nm}^0|^2 [\psi'_n(s_c z)]^* \psi_n(s_c z)) \right\}. \quad (28)$$

In our case of a two-layer EMM, there is no absorption in the spacer layer and the absorption inside the anisotropic shell can then be computed as

$$C_{\text{abs}}^{\text{Shell}} = C_{\text{abs}} - C_{\text{abs}}^{\text{Core}}, \quad (29)$$

where C_{abs} is the total absorption cross section, which in this case can either be computed from Eq. (27) ($j = 2$) or from Eq. (4). The second expression is simpler, but we checked that both give the same result.

The TASA can be used to compute $C_{\text{abs}}^{\text{Shell}}$ without the need for complex-order Bessel functions. This can be done using Eqs. (29) and (28) with coefficients α_{nm}^0 and β_{nm}^0 as given in Appendix C. As illustrated in Fig. 3, the TASA solution for the internal absorption of the core $C_{\text{abs}}^{\text{Core}}$ [Fig. 3(a)] and the shell $C_{\text{abs}}^{\text{Shell}}$ [Figs. 3(b) to 3(c)] again agrees well with the full solution.

It is worth reemphasizing that the shell internal absorption is not identical to the differential absorption cross section and this is shown explicitly in Figs. 3(b) and 3(c) where the two are compared for the two dye orientations (perpendicular and parallel). The peaks in $\delta C_{\text{abs}}^{\text{Shell}}$ can be interpreted as surface-enhanced absorption. The main peak at 526 nm is the original dye peak. The shoulder at 430 nm and small peak at 370 nm correspond to enhanced absorption at the nanoparticle dipolar and quadrupolar plasmon resonance. The dye absorption is normally small there, but is nevertheless enhanced as a result of enhanced local field at these resonances [11]. $\delta C_{\text{abs}}^{\text{Core}}$ is dominated by the plasmon resonance peaks, but more interesting effects are visible when subtracting the cross section of the bare NP only, which reveals the effect of the dye layer on the core absorption. A derivative-like spectral shape is observed around the quadrupolar resonance (for $\delta C_{\text{abs}}^{\text{Core}}$). This is attributed to the quadrupolar plasmon resonance shift

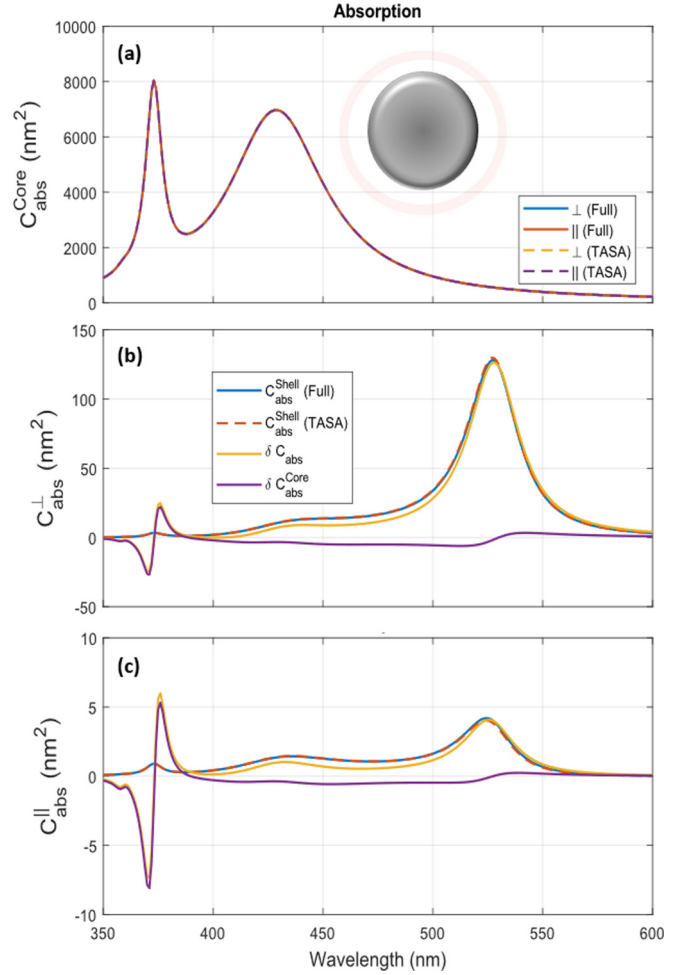


FIG. 3. (a) Internal absorption cross section inside the silver sphere $C_{\text{abs}}^{\text{Core}}$ for two dye orientations, perpendicular (\perp) and tangential (\parallel). The TASA and full solutions are compared. (b,c) Corresponding internal absorption in the shell $C_{\text{abs}}^{\text{Shell}}$ in the full and TASA solutions for (b) \perp and (c) \parallel dye orientations. These are compared to the differential core absorption $\delta C_{\text{abs}}^{\text{Core}}$ and the standard differential absorption cross-section δC_{abs} discussed earlier. Note that $\delta C_{\text{abs}} = \delta C_{\text{abs}}^{\text{Core}} + C_{\text{abs}}^{\text{Shell}}$.

induced by the presence of the dye layer. We note that this shift appears larger in magnitude for perpendicular dye orientation. Such shifts of the plasmon resonance as a function of the external dielectric medium are expected [11, 14]. However, the influence of dye orientations on these shifts had not been discussed. A more detailed discussion is, however, outside the scope of the present work.

VI. CONCLUSION

We derived expressions for the Mie coefficients of the two-layer EMM scattering problem in the thin-shell approximation. We checked the validity of this approximation against the full anisotropic Mie solutions and shown that it is accurate for dye-on-NP systems, much more so than the single-layer EMM. The main advantage of this thin shell approximation is that the solution does not require the computation of Bessel functions of complex order, which will simplify further

analytical development and speed up numerical calculations. We also illustrated the usefulness of this work by calculating the internal absorption cross sections inside the shell and the core, individually. This study was focused on the optical properties of a system consisting of a particle coated with a (sub)monolayer of molecules, where the thin-shell approximation is particularly suited, but we believe the TASA could also prove useful for a particle surrounded by small particles (core-satellites system). For the approximation to remain valid for such a thicker shell, it may be required to include second or higher orders of the Taylor approximation as in Ref. [44]. Overall, this work complements our recent development of an effective medium model for dyes adsorbed on NPs [32] and will simplify its implementation and uptake for calculations of their optical properties, for example, to study the influence of adsorbate orientation effects on plasmon resonances.

ACKNOWLEDGMENTS

The authors are grateful for support from the Royal Society Te Apārangi New Zealand (Rutherford Discovery Fellowship, B.A.) and from the MacDiarmid institute of Advanced Materials and Nanotechnology.

APPENDIX A: FULL ANISOTROPIC MIE SOLUTIONS

We first write down the electric fields expansions in terms of vector spherical harmonics (VSHs) [43] for the incident field, scattered field, and internal fields in the core, spacer, and shell, respectively,

$$\begin{aligned}\mathbf{E}_{\text{inc}} &= E_0 \sum_{n,m} a_{nm} \mathbf{M}_{nm}^{(1)}(k_m \mathbf{r}) + b_{nm} \mathbf{N}_{nm}^{(1)}(k_m \mathbf{r}), \\ \mathbf{E}_{\text{Sca}} &= E_0 \sum_{n,m} p_{nm} \mathbf{M}_{nm}^{(3)}(k_m \mathbf{r}) + q_{nm} \mathbf{N}_{nm}^{(3)}(k_m \mathbf{r}), \\ \mathbf{E}_{\text{C}} &= E_0 \sum_{n,m} \alpha_{nm}^0 \mathbf{M}_{nm}^{(1)}(k_{\text{in}} \mathbf{r}) + \beta_{nm}^0 \mathbf{N}_{nm}^{(1)}(k_{\text{in}} \mathbf{r}), \\ \mathbf{E}_{\text{Gap}} &= E_0 \sum_{n,m} \alpha_{nm}^1 \mathbf{M}_{nm}^{(1)}(k_m \mathbf{r}) + \beta_{nm}^1 \mathbf{N}_{nm}^{(1)}(k_m \mathbf{r}) \\ &\quad + \gamma_{nm}^1 \mathbf{M}_{nm}^{(2)}(k_m \mathbf{r}) + \delta_{nm}^1 \mathbf{N}_{nm}^{(2)}(k_m \mathbf{r}), \\ \mathbf{E}_{\text{Sh}} &= \frac{\varepsilon}{\varepsilon_t} E_0 \sum_{n,m} \alpha_{nm}^2 \mathbf{M}_{nm}^{(1)}(k_t \mathbf{r}) + \beta_{nm}^2 \tilde{\mathbf{N}}_{nm}^{(1)}(k_t \mathbf{r}) \\ &\quad + \gamma_{nm}^2 \mathbf{M}_{nm}^{(2)}(k_t \mathbf{r}) + \delta_{nm}^2 \tilde{\mathbf{N}}_{nm}^{(2)}(k_t \mathbf{r}).\end{aligned}$$

Their corresponding magnetic fields expansions can be found as $\mathbf{H} = (\nabla \times \mathbf{E})/i\omega\mu$. Note the presence of complex order VSHs, $\tilde{\mathbf{N}}_{nm}^{(i)}$, for the shell expansion to account for the anisotropy. The boundary conditions at $r = a$ mean that the

tangential components of \mathbf{E}_{Gap} , \mathbf{H}_{Gap} are equal to those of \mathbf{E}_{C} , \mathbf{H}_{C} , respectively. This gives

$$\alpha_{nm}^1 \psi_n(z) + \gamma_{nm}^1 \chi_n(z) = \alpha_{nm}^0 \psi_n(s_{\text{in}} z)/s_{\text{in}}, \quad (\text{A1})$$

$$\beta_{nm}^1 \psi'_n(z) + \delta_{nm}^1 \chi'_n(z) = \beta_{nm}^0 \psi'_n(s_{\text{in}} z)/s_{\text{in}}, \quad (\text{A2})$$

$$\alpha_{nm}^1 \psi'_n(z) + \gamma_{nm}^1 \chi'_n(z) = \alpha_{nm}^0 \psi'_n(s_{\text{in}} z), \quad (\text{A3})$$

$$\alpha_{nm}^1 \psi_n(z) + \delta_{nm}^1 \chi_n(z) = \beta_{nm}^0 \psi_n(s_{\text{in}} z), \quad (\text{A4})$$

where $s_{\text{in}} = \sqrt{\varepsilon_{\text{in}}}/\sqrt{\varepsilon_{\text{m}}}$, $z = k_m a$. From these, we deduce

$$\frac{\gamma_{nm}^1}{\alpha_{nm}^1} = -\frac{s_{\text{in}} \psi_n(z) \psi'_n(s_{\text{in}} z) - \psi_n(z) \psi'_n(s_{\text{in}} z)}{s_{\text{in}} \chi_n(z) \psi'_n(s_{\text{in}} z) - \chi_n(z) \psi'_n(s_{\text{in}} z)} \equiv \Gamma_n^{(1)}, \quad (\text{A5})$$

$$\frac{\delta_{nm}^1}{\beta_{nm}^1} = -\frac{s_{\text{in}} \psi'_n(z) \psi_n(s_{\text{in}} z) - \psi'_n(z) \psi_n(s_{\text{in}} z)}{s_{\text{in}} \chi'_n(z) \psi_n(s_{\text{in}} z) - \chi'_n(z) \psi_n(s_{\text{in}} z)} \equiv \Delta_n^{(1)}. \quad (\text{A6})$$

Similarly, the boundary conditions at $r = b$ give

$$[\alpha_{nm}^2 \psi_n(s_t y) + \gamma_{nm}^2 \chi_n(s_t y)]/s_t = \alpha_{nm}^1 \psi_n(y) + \gamma_{nm}^1 \chi_n(y), \quad (\text{A7})$$

$$[\beta_{nm}^2 \tilde{\psi}'_n(s_t y) + \delta_{nm}^2 \tilde{\chi}'_n(s_t y)]/s_t = \beta_{nm}^1 \psi'_n(y) + \delta_{nm}^1 \chi'_n(y), \quad (\text{A8})$$

$$\alpha_{nm}^2 \psi'_n(s_t y) + \gamma_{nm}^2 \chi'_n(s_t y) = \alpha_{nm}^1 \psi'_n(y) + \beta_{nm}^1 \chi'_n(y), \quad (\text{A9})$$

$$\beta_{nm}^2 \tilde{\psi}_n(s_t y) + \delta_{nm}^2 \tilde{\chi}_n(s_t y) = \beta_{nm}^1 \psi_n(y) + \delta_{nm}^1 \chi_n(y), \quad (\text{A10})$$

where $s_t = \sqrt{\varepsilon_t}/\sqrt{\varepsilon_{\text{m}}}$, $y = k_m b$. These lead to

$$\frac{\gamma_{nm}^2}{\alpha_{nm}^2} = -\frac{[\psi \psi]_{n,y}^{m,s} + \Gamma_n^{(1)} [\psi \chi]_{n,y}^{m,s}}{[\chi \psi]_{n,y}^{m,s} + \Gamma_n^{(1)} [\chi \chi]_{n,y}^{m,s}} \equiv \Gamma_n^{(2)}, \quad (\text{A11})$$

$$\frac{\delta_{nm}^2}{\beta_{nm}^2} = -\frac{[\psi \psi]_{n,y}^{e,s} + \Delta_n^{(1)} [\psi \chi]_{n,y}^{e,s}}{[\chi \psi]_{n,y}^{e,s} + \Delta_n^{(1)} [\chi \chi]_{n,y}^{e,s}} \equiv \Delta_n^{(2)}. \quad (\text{A12})$$

The boundary conditions at $r = c$ involve the incident and scattered field on the outside and give

$$a_{nm} \psi_n(x) + p_{nm} \xi_n(x) = [\alpha_{nm}^2 \psi_n(s_t x) + \gamma_{nm}^2 \chi_n(s_t x)]/s_t, \quad (\text{A13})$$

$$b_{nm} \psi'_n(x) + q_{nm} \xi'_n(x) = [\beta_{nm}^2 \tilde{\psi}'_n(s_t x) + \delta_{nm}^2 \tilde{\chi}'_n(s_t x)]/s_t, \quad (\text{A14})$$

$$a_{nm} \psi'_n(x) + p_{nm} \xi'_n(x) = \alpha_{nm}^2 \psi'_n(s_t x) + \gamma_{nm}^2 \chi'_n(s_t x), \quad (\text{A15})$$

$$b_{nm} \psi_n(x) + q_{nm} \xi_n(x) = \beta_{nm}^2 \tilde{\psi}_n(s_t x) + \delta_{nm}^2 \tilde{\chi}_n(s_t x), \quad (\text{A16})$$

where $x = k_m c$. These lead to

$$\Gamma_n = -\frac{[\psi \psi]_{n,x}^{m,s} + \Gamma_n^{(2)} [\chi \psi]_{n,x}^{m,s}}{[\psi \xi]_{n,x}^{m,s} + \Gamma_n^{(2)} [\chi \xi]_{n,x}^{m,s}}, \quad (\text{A17})$$

$$\Delta_n = -\frac{[\psi \psi]_{n,x}^{e,s} + \Delta_n^{(2)} [\chi \psi]_{n,x}^{e,s}}{[\psi \xi]_{n,x}^{e,s} + \Delta_n^{(2)} [\chi \xi]_{n,x}^{e,s}}, \quad (\text{A18})$$

and substituting Eqs. (A11) to (A12), we obtain

$$\Gamma_n = \frac{p_{nm}}{a_{nm}} = -\frac{[\psi \psi]_{n,x}^{m,s} ([\chi \psi]_{n,y}^{m,s} + \Gamma_n^{(1)} [\chi \chi]_{n,y}^{m,s}) - [\chi \psi]_{n,x}^{m,s} ([\psi \psi]_{n,y}^{m,s} + \Gamma_n^{(1)} [\psi \chi]_{n,y}^{m,s})}{[\psi \xi]_{n,x}^{m,s} ([\chi \psi]_{n,y}^{m,s} + \Gamma_n^{(1)} [\chi \chi]_{n,y}^{m,s}) - [\chi \xi]_{n,x}^{m,s} ([\psi \psi]_{n,y}^{m,s} + \Gamma_n^{(1)} [\psi \chi]_{n,y}^{m,s})} \equiv -\frac{N_{1n}}{D_{1n}}, \quad (\text{A19})$$

$$\Delta_n = \frac{q_{nm}}{b_{nm}} = -\frac{[\psi \psi]_{n,x}^{e,s} ([\chi \psi]_{n,y}^{e,s} + \Delta_n^{(1)} [\chi \chi]_{n,y}^{e,s}) - [\chi \psi]_{n,x}^{e,s} ([\psi \psi]_{n,y}^{e,s} + \Delta_n^{(1)} [\psi \chi]_{n,y}^{e,s})}{[\psi \xi]_{n,x}^{e,s} ([\chi \psi]_{n,y}^{e,s} + \Delta_n^{(1)} [\chi \chi]_{n,y}^{e,s}) - [\chi \xi]_{n,x}^{e,s} ([\psi \psi]_{n,y}^{e,s} + \Delta_n^{(1)} [\psi \chi]_{n,y}^{e,s})} \equiv -\frac{N_{2n}}{D_{2n}}. \quad (\text{A20})$$

APPENDIX B: THIN-ANISOTROPIC-SHELL APPROXIMATION

1. Useful identities

The first two useful identities are the relationships (differential equations) between the generalized Riccati-Bessel functions and their second derivatives, which are obtained by Lange and Aragón (Eqs. (A9) and (A10) in Ref. [35]) as

$$\Xi_n'' + \left[1 - \frac{n(n+1)}{x^2} \right] \Xi_n = 0, \quad (\text{B1})$$

$$\tilde{\Xi}_n'' + \left[1 - \frac{\varepsilon_t}{\varepsilon_n} \frac{n(n+1)}{x^2} \right] \tilde{\Xi}_n = 0, \quad (\text{B2})$$

where Ξ represents all types of the Riccati-Bessel functions ψ , χ , and ξ . Other useful identities are

$$[\psi \Omega]_{n,y}^{e,s} \tilde{\chi}_n(s_t y) - [\chi \Omega]_{n,y}^{e,s} \tilde{\psi}_n(s_t y) = \Omega_n(y), \quad (\text{B3})$$

$$[\psi \Omega]_{n,y}^{e,s} \tilde{\chi}'_n(s_t y) - [\chi \Omega]_{n,y}^{e,s} \tilde{\psi}'_n(s_t y) = s_t \Omega'_n(y), \quad (\text{B4})$$

$$[\psi \Omega]_{n,y}^{m,s} \chi_n(s_t y) - [\chi \Omega]_{n,y}^{m,s} \psi_n(s_t y) = -s_t \Omega_n(y), \quad (\text{B5})$$

$$[\psi \Omega]_{n,y}^{m,s} \chi'_n(s_t y) - [\chi \Omega]_{n,y}^{m,s} \psi'_n(s_t y) = -\Omega'_n(y), \quad (\text{B6})$$

$$[\psi \Omega]_{n,y}^{e,c} \tilde{\chi}_n(s_t y) - [\chi \Omega]_{n,y}^{e,c} \tilde{\psi}_n(s_t y) = -s_{in} \Omega_n(s_{in} y), \quad (\text{B7})$$

$$[\psi \Omega]_{n,y}^{e,c} \tilde{\chi}'_n(s_t y) - [\chi \Omega]_{n,y}^{e,c} \tilde{\psi}'_n(s_t y) = -s_t \Omega'_n(s_{in} y), \quad (\text{B8})$$

$$[\psi \Omega]_{n,y}^{m,c} \chi_n(s_t y) - [\chi \Omega]_{n,y}^{m,c} \psi_n(s_t y) = s_t \Omega_n(s_{in} y), \quad (\text{B9})$$

$$[\psi \Omega]_{n,y}^{m,c} \chi'_n(s_t y) - [\chi \Omega]_{n,y}^{m,c} \psi'_n(s_t y) = s_{in} \Omega'_n(s_{in} y), \quad (\text{B10})$$

where Ω denotes ψ or ξ and the brackets $[\]$ are defined in Eq. (13) in the main text. The first expression, Eq. (B3), can be easily proven as follows

$$\begin{aligned} [\psi \Omega]_{n,y}^{e,s} \tilde{\chi}_n(s_t y) - [\chi \Omega]_{n,y}^{e,s} \tilde{\psi}_n(s_t y) &= \{s_t \tilde{\psi}_n(s_t y) \Omega'_n(y) - \tilde{\psi}'_n(s_t y) \Omega_n(y)\} \tilde{\chi}_n(s_t y) - \{s_t \tilde{\chi}_n(s_t y) \Omega'_n(y) - \tilde{\chi}'_n(s_t y) \Omega_n(y)\} \tilde{\psi}_n(s_t y) \\ &= s_t \Omega'_n(y) \{ \tilde{\psi}_n(s_t y) \tilde{\chi}_n(s_t y) - \tilde{\chi}_n(s_t y) \tilde{\psi}_n(s_t y) \} - \Omega_n(y) \{ \tilde{\psi}'_n(s_t y) \tilde{\chi}_n(s_t y) - \tilde{\chi}'_n(s_t y) \tilde{\psi}_n(s_t y) \} \\ &= \Omega_n(y), \end{aligned}$$

where for the last equality, we apply the Wronskian identity of the Riccati-Bessel function of the complex order [40], $\tilde{\psi}_n \tilde{\chi}'_n - \tilde{\psi}'_n \tilde{\chi}_n = 1$. The other expressions, Eqs. (B4) to (B10), can be proven in a similar fashion.

2. TASA Solution of the two-layer stratified sphere

We first define $\delta = x - y = k_m l_s$ and search for an approximation in the limit $\delta \ll x, y$. Taylor expansion to the first order in δ leads to

$$\Gamma_n(y, \delta) = -\frac{N_{1n}}{D_{1n}} - \delta \left(\frac{N'_{1n} D_{1n} - N_{1n} D'_{1n}}{(D_{1n})^2} \right), \quad (\text{B11})$$

$$\Delta_n(y, \delta) = -\frac{N_{2n}}{D_{2n}} - \delta \left(\frac{N'_{2n} D_{2n} - N_{2n} D'_{2n}}{(D_{2n})^2} \right). \quad (\text{B12})$$

We first focus on Δ_n . We need to find the terms $N_{2n}|_{x=y}$, $D_{2n}|_{x=y}$, $N'_{2n}|_{x=y}$, and $D'_{2n}|_{x=y}$ to find the TASA expression for $\Delta_n(\delta)$. Using the useful identities given above, we obtain

$$N_{2n}|_{x=y} = [\psi \psi]_{n,y}^{e,s} ([\chi \psi]_{n,y}^{e,s} + \Delta_n^{(1)} [\chi \chi]_{n,y}^{e,s}) - [\chi \psi]_{n,y}^{e,s} ([\psi \psi]_{n,y}^{e,s} + \Delta_n^{(1)} [\psi \chi]_{n,y}^{e,s}) \quad (\text{B13})$$

$$\begin{aligned} &= \Delta_n^{(1)} [\psi \psi]_{n,y}^{e,s} \{s_t \tilde{\chi}_n(s_t y) \chi'_n(y) - \tilde{\chi}'_n(s_t y) \chi_n(y)\} - \Delta_n^{(1)} [\chi \psi]_{n,y}^{e,s} \{s_t \tilde{\psi}_n(s_t y) \chi'_n(y) - \tilde{\psi}'_n(s_t y) \chi_n(y)\} \\ &= \Delta_n^{(1)} \{s_t \psi_n(y) \chi'_n(y) - s_t \psi'_n(y) \chi_n(y)\} \\ &= s_t \Delta_n^{(1)}. \end{aligned} \quad (\text{B14})$$

From second to third equality, we used Eqs. (B3) and (B4). For the last equality, the Wronskian identity of the Riccati-Bessel function was used $\psi \chi' - \psi' \chi = 1$, which leads to $\xi \chi' - \xi' \chi = 1$ and $\psi \xi' - \psi' \xi = i$. Similarly, the denominator can be found

as

$$D_{2n}|_{x=y} = s_t(\Delta_n^{(1)} - i). \quad (\text{B15})$$

Then, using Eqs. (B1) and (B2), we can write the derivatives of the numerator and denominator as

$$\begin{aligned} N'_{2n}|_{x=y} &= \left[\frac{s_t n(n+1)}{y^2} \left(1 - \frac{\varepsilon_t}{\varepsilon_n s_t^2} \right) \tilde{\psi}_n(s_t y) \psi_n(y) + (s_t^2 - 1) \tilde{\psi}'_n(s_t y) \psi'_n(y) \right] ([\chi \psi]_{n,y}^{e,s} + \Delta_n^{(1)} [\chi \chi]_{n,y}^{e,s}) \\ &\quad - \left[\frac{s_t n(n+1)}{y^2} \left(1 - \frac{\varepsilon_t}{\varepsilon_n s_t^2} \right) \tilde{\chi}_n(s_t y) \psi_n(y) + (s_t^2 - 1) \tilde{\chi}'_n(s_t y) \psi'_n(y) \right] ([\psi \chi]_{n,y}^{e,s} + \Delta_n^{(1)} [\psi \psi]_{n,y}^{e,s}) \\ &= \frac{s_t n(n+1)}{y^2} \left(\frac{\varepsilon_t}{\varepsilon_n s_t^2} - 1 \right) \psi_n(y) [\psi_n(y) + \Delta_n^{(1)} \chi_n(y)] + s_t (1 - s_t^2) \psi'_n(y) [\psi'_n(y) + \Delta_n^{(1)} \chi'_n(y)], \end{aligned} \quad (\text{B16})$$

$$D'_{2n}|_{x=y} = \frac{s_t n(n+1)}{y^2} \left(\frac{\varepsilon_t}{\varepsilon_n s_t^2} - 1 \right) \xi_n(y) [\psi_n(y) + \Delta_n^{(1)} \chi_n(y)] + s_t (1 - s_t^2) \xi'_n(y) [\psi'_n(y) + \Delta_n^{(1)} \chi'_n(y)]. \quad (\text{B17})$$

The same approach can be applied to get all the terms for $\Gamma_n(\delta)$.

APPENDIX C: INTERNAL ABSORPTION

To compute the internal absorption inside the core and the shell, separately, we need the coefficients α_{nm}^0 and β_{nm}^0 . We shall first derive the expression for β_{nm}^0 . Equations (A14) and (A16) give

$$\frac{\beta_{nm}^2}{b_{nm}} = - [s_t \psi'_n(x) \tilde{\chi}_n(s_t x) - \psi_n(x) \tilde{\chi}'_n(s_t x)] - \Delta_n [s_t \xi'_n(x) \tilde{\chi}_n(s_t x) - \xi_n(x) \tilde{\chi}'_n(s_t x)], \quad (\text{C1})$$

$$\frac{\delta_{nm}^2}{b_{nm}} = [s_t \psi'_n(x) \tilde{\psi}_n(s_t x) - \psi_n(x) \tilde{\psi}'_n(s_t x)] + \Delta_n [s_t \xi'_n(x) \tilde{\psi}_n(s_t x) - \xi_n(x) \tilde{\psi}'_n(s_t x)]. \quad (\text{C2})$$

In the limit of $x \rightarrow y$ (thin-shell approximation), the Taylor expansions are

$$\frac{\beta_{nm}^2}{b_{nm}}(\delta) = \frac{\beta_{nm}^2}{b_{nm}} \Big|_{x=y} + \delta \frac{\partial}{\partial x} \left(\frac{\beta_{nm}^2}{b_{nm}} \right) \Big|_{x=y}, \quad (\text{C3})$$

$$\frac{\delta_{nm}^2}{b_{nm}}(\delta) = \frac{\delta_{nm}^2}{b_{nm}} \Big|_{x=y} + \delta \frac{\partial}{\partial x} \left(\frac{\delta_{nm}^2}{b_{nm}} \right) \Big|_{x=y}, \quad (\text{C4})$$

where the first derivative of these coefficients can be found as

$$\frac{\partial}{\partial x} \left(\frac{\beta_{nm}^2}{b_{nm}} \right) = - \frac{s_t n(n+1)}{x^2} \left(1 - \frac{\varepsilon_t}{\varepsilon_n s_t^2} \right) [\psi_n(x) + \Delta_n \xi_n(x)] \tilde{\chi}_n(s_t x) - (s_t^2 - 1) [\psi'_n(x) + \Delta_n \xi'_n(x)] \tilde{\chi}'_n(s_t x), \quad (\text{C5})$$

$$\frac{\partial}{\partial x} \left(\frac{\delta_{nm}^2}{b_{nm}} \right) = \frac{s_t n(n+1)}{x^2} \left(1 - \frac{\varepsilon_t}{\varepsilon_n s_t^2} \right) [\psi_n(x) + \Delta_n \xi_n(x)] \tilde{\psi}_n(s_t x) + (s_t^2 - 1) [\psi'_n(x) + \Delta_n \xi'_n(x)] \tilde{\psi}'_n(s_t x). \quad (\text{C6})$$

Therefore, Eqs. (A8) and (A10) become

$$b_{nm}[\psi'_n(y) + \Delta_n \xi'_n(y) + \mathcal{F}_1] = \beta_{nm}^1 \psi'_n(y) + \delta_{nm}^1 \chi'_n(y), \quad (\text{C7})$$

$$b_{nm}[\psi_n(y) + \Delta_n \xi_n(y) + \mathcal{F}_2] = \beta_{nm}^1 \psi_n(y) + \delta_{nm}^1 \chi_n(y), \quad (\text{C8})$$

where

$$\mathcal{F}_1 = \delta \frac{n(n+1)}{y^2} \left(1 - \frac{\varepsilon_t}{\varepsilon_n s_t^2} \right) [\psi_n(y) + \Delta_n \xi_n(y)], \quad (\text{C9})$$

$$\mathcal{F}_2 = \delta (1 - s_t^2) [\psi'_n(y) + \Delta_n \xi'_n(y)]. \quad (\text{C10})$$

From Eqs. (C7) and (C8), we can then express β_{nm}^1 and δ_{nm}^1 as

$$\frac{\beta_{nm}^1}{b_{nm}} = 1 + \Delta_n + [\mathcal{F}_2 \chi'_n(y) - \mathcal{F}_1 \chi_n(y)], \quad (\text{C11})$$

$$\frac{\delta_{nm}^1}{b_{nm}} = i \Delta_n + [\mathcal{F}_1 \psi_n(y) - \mathcal{F}_2 \psi'_n(y)]. \quad (\text{C12})$$

We can then rearrange one of the Eqs. (A2) or (A4) to deduce the TASA for the internal coefficient β_{nm}^0 :

$$\beta_{nm}^0 = s_{\text{in}} \frac{\beta_{nm}^1 \psi'_n(z) + \delta_{nm}^1 \xi'_n(z)}{\psi'_n(s_{\text{in}} z)} = \frac{\beta_{nm}^1 \psi_n(z) + \delta_{nm}^1 \xi_n(z)}{\psi_n(s_{\text{in}} z)}. \quad (\text{C13})$$

A similar procedure can be followed to get α_{nm}^0 , giving

$$\frac{\alpha_{nm}^1}{a_{nm}} = 1 + \Gamma_n, \quad \frac{\gamma_{nm}^1}{a_{nm}} = i \Gamma_n, \quad (\text{C14})$$

which leads to

$$\frac{\alpha_{nm}^0}{a_{nm}} = \frac{\psi'_n(z) + \Gamma_n \xi'_n(z)}{\psi'_n(s_{\text{in}} z)} = s_{\text{in}} \frac{\psi_n(z) + \Gamma_n \xi_n(z)}{\psi_n(s_{\text{in}} z)}. \quad (\text{C15})$$

These TASA expressions for α_{nm}^0 and β_{nm}^0 are in terms of the incident coefficients and they do not require the calculations of complex-ordered Bessel functions.

- [1] G. Mie, Contributions to the optics of turbid media, particularly of colloidal metal solutions, *Ann. Phys. (Leipzig)* **25**, 377 (1908).
- [2] C. F. Bohren and D. R. Huffman, *Absorption and Scattering of Light by Small Particles* (John Wiley & Sons, New York, 2008).
- [3] A. L. Aden and M. Kerker, Scattering of electromagnetic waves from two concentric spheres, *J. Appl. Phys.* **22**, 1242 (1951).
- [4] D. Schebarchov, B. Auguie, and E. C. Le Ru, Simple accurate approximations for the optical properties of metallic nanospheres and nanoshells, *Phys. Chem. Chem. Phys.* **15**, 4233 (2013).
- [5] S. A. Maier, *Plasmonics: Fundamentals and Applications* (Springer Science & Business Media, New York, 2007).
- [6] T. W. Odom and G. C. Schatz, Introduction to plasmonics, *Chem. Rev.* **111**, 3667 (2011).
- [7] J. N. Anker, W. P. Hall, O. Lyandres, N. C. Shah, J. Zhao, and R. P. Van Duyne, Biosensing with plasmonic nanosensors, *Nat. Mater.* **7**, 442 (2008).
- [8] W. C. Law, K. T. Yong, A. Baev, and P. N. Prasad, Sensitivity improved surface plasmon resonance biosensor for cancer biomarker detection based on plasmonic enhancement, *ACS Nano* **5**, 4858 (2011).
- [9] S. Zhang, R. Geryak, J. Geldmeier, S. Kim, and V. V. Tsukruk, Synthesis, assembly, and applications of hybrid nanostructures for biosensing, *Chem. Rev.* **117**, 12942 (2017).
- [10] B. S. Hoener, S. R. Kirchner, T. S. Heiderscheidt, S. S. Collins, W. S. Chang, S. Link, and C. F. Landes, Plasmonic sensing and control of single-nanoparticle electrochemistry, *Chem.* **4**, 1560 (2018).
- [11] E. C. Le Ru and P. G. Etchegoin, *Principles of Surface-Enhanced Raman Spectroscopy: and Related Plasmonic Effects* (Elsevier, New York, 2009).
- [12] W. Ni, T. Ambjornsson, S. P. Apell, H. Chen, and J. Wang, Observing plasmonic-molecular resonance coupling on single gold nanorods, *Nano Lett.* **10**, 77 (2010).
- [13] W. Ni, H. Chen, J. Su, Z. Sun, J. Wang, and H. Wu, Effects of dyes, gold nanocrystals, pH, and metal ions on plasmonic and molecular resonance coupling, *J. Am. Chem. Soc.* **132**, 4806 (2010).
- [14] J. Zhao, L. Jensen, J. Sung, S. Zou, G. C. Schatz, and R. P. Van Duyne, Interaction of plasmon and molecular resonances for rhodamine 6G adsorbed on silver nanoparticles, *J. Am. Chem. Soc.* **129**, 7647 (2007).
- [15] J.-Y. Yan, W. Zhang, S. Duan, X.-G. Zhao, and A. O. Govorov, Optical properties of coupled metal-semiconductor and metal-molecule nanocrystal complexes: Role of multipole effects, *Phys. Rev. B* **77**, 165301 (2008).
- [16] N. T. Fofang, T. Park, O. Neumann, N. A. Mirin, P. Nordlander, and N. J. Halas, Plexcitonic nanoparticles: Plasmon-exciton coupling in nanoshell-J-aggregate complexes, *Nano Lett.* **8**, 3481 (2008).
- [17] T. J. Antosiewicz, S. P. Apell, and T. Shegai, Plasmon-exciton interactions in a core-shell geometry: From enhanced absorption to strong coupling, *ACS Photonics* **1**, 454 (2014).
- [18] A. O. Cacciola, O. Di Stefano, R. Stassi, R. Saija, and S. Savasta, Ultrastrong coupling of plasmons and excitons in a nanoshell, *ACS Nano* **8**, 11483 (2014).
- [19] B. L. Darby, B. Auguie, M. Meyer, A. E. Pantoja, and E. C. Le Ru, Modified optical absorption of molecules on metallic nanoparticles at sub-monolayer coverage, *Nat. Photon.* **10**, 40 (2016).
- [20] A. M. Fales, S. J. Norton, B. M. Crawford, B. G. DeLacy, and T. Vo-Dinh, Fano resonance in a gold nanosphere with a J-aggregate coating, *Phys. Chem. Chem. Phys.* **17**, 24931 (2015).
- [21] R. Chikkaraddy, B. de Nijs, F. Benz, S. J. Barrow, O. A. Scherman, E. Rosta, A. Demetriadou, P. Fox, O. Hess, and J. J. Baumberg, Single-molecule strong coupling at room temperature in plasmonic nanocavities, *Nature (London)* **535**, 127 (2016).
- [22] G. Zengin, T. Gschneidner, R. Verre, L. Shao, T. J. Antosiewicz, K. Moth-Poulsen, M. Käll, and T. Shegai, Evaluating conditions for strong coupling between nanoparticle plasmons and organic dyes using scattering and absorption spectroscopy, *J. Phys. Chem. C* **120**, 20588 (2016).
- [23] J. Jin, *The Finite Element Method in Electromagnetics*, 2nd ed., (Wiley-IEEE, New York, 2002).
- [24] J. Grand and E. C. Le Ru, Practical implementation of accurate finite-element calculations for electromagnetic scattering by nanoparticles, *Plasmonics* **15**, 109 (2020).
- [25] C. W. Qiu, L. Gao, J. D. Joannopoulos, and M. Soljačić, Light scattering from anisotropic particles: propagation, localization, and nonlinearity, *Laser Photonics Rev.* **4**, 268 (2010).
- [26] H. Wallén, H. Kettunen, and A. Sihvola, Anomalous absorption, plasmonic resonances, and invisibility of radially anisotropic spheres, *Radio Sci.* **50**, 18 (2015).
- [27] M. Moskovits, Surface selection rules, *J. Chem. Phys.* **77**, 4408 (1982).
- [28] E. C. Le Ru, S. A. Meyer, C. Artur, P. G. Etchegoin, J. Grand, P. Lang, and F. Maurel, Experimental demonstration of surface selection rules for SERS on flat metallic surfaces, *Chem. Comm.* **47**, 3903 (2011).
- [29] J. Roth and M. J. Dignam, Scattering and extinction cross sections for a spherical particle coated with an oriented molecular layer, *J. Opt. Soc. Am.* **63**, 308 (1973).
- [30] A. Bagchi, R. G. Barrera, and B. B. Dasgupta, Classical Local-Field Effect in Reflectance from Adsorbed Overlayers, *Phys. Rev. Lett.* **44**, 1475 (1980).
- [31] A. Bagchi, R. G. Barrera, and R. Fuchs, Local-field effect in optical reflectance from adsorbed overlayers, *Phys. Rev. B* **25**, 7086 (1982).
- [32] C. Tang, B. Auguie, and E. C. Le Ru, Refined effective-medium model for the optical properties of nanoparticles coated with anisotropic molecules, *Phys. Rev. B* **103**, 085436 (2021).
- [33] B. Auguie, B. L. Darby, and E. C. Le Ru, Electromagnetic interactions of dye molecules surrounding a nanosphere, *Nanoscale* **11**, 12177 (2019).
- [34] B. Auguie and E. C. Le Ru, Optical absorption of dye molecules in a spherical shell geometry, *J. Phys. Chem. C* **122**, 19110 (2018).
- [35] B. Lange and S. R. Aragón, Mie scattering from thin anisotropic spherical shells, *J. Chem. Phys.* **92**, 4643 (1990).
- [36] C. Tang, B. Auguie, and E. C. Le Ru, Modeling molecular orientation effects in dye-coated nanostructures using a thin-shell approximation of mie theory for radially anisotropic media, *ACS Photonics* **5**, 5002 (2018).

- [37] C. M. Galloway, C. Artur, J. Grand, and E. C. Le Ru, Photobleaching of fluorophores on the surface of nanoantennas, *J. Phys. Chem. C* **118**, 28820 (2014).
- [38] K. Li, N. J. Hogan, M. J. Kale, N. J. Halas, P. Nordlander, and P. Christopher, Balancing near-field enhancement, absorption, and scattering for effective antenna-reactor plasmonic photocatalysis, *Nano Lett* **17**, 3710 (2017).
- [39] D. W. Mackowski, R. A. Altenkirch, and M. P. Menguc, Internal absorption cross sections in a stratified sphere, *Appl. Opt.* **29**, 1551 (1990).
- [40] M. Abramowitz and I. A. Stegun, *Handbook of Mathematical Functions: With Formulas, Graphs, and Mathematical Tables*, Vol. 55, (Courier Corporation, North Chelmsford, MA, 1965).
- [41] P. Godfrey, Gamma, MATLAB Central File Exchange: <https://www.mathworks.com/matlabcentral/fileexchange/3572-gamma>, [Online; accessed 31-May-2021].
- [42] A. Djorović, M. Meyer, B. L. Darby, and E. C. Le Ru, Accurate modeling of the polarizability of dyes for electromagnetic calculations, *ACS Omega* **2**, 1804 (2017).
- [43] M. I. Mishchenko, L. D. Travis, and A. A. Lacis, *Scattering, Absorption, and Emission of Light by Small Particles* (Cambridge University Press, Cambridge, England, 2002).
- [44] D. K. Hahn and S. R. Aragón, Mie scattering from anisotropic thick spherical shells, *J. Chem. Phys.* **101**, 8409 (1994).